Paper

Modeling and Estimating of the Fluorescent Lamp and Its Pre-heating Control

Guan-Chyun HSIEH and Chang-Hua LIN

Department of Electronic Engineering
National Taiwan University of Science and Technology
Taipei, Taiwan 106, R. O. C.

Received December. 17, 1997.

ABSTRACT

This paper explores the characteristic of the fluorescent lamp operating in high-frequency range. The fluorescent lamp actually characterizes an impedance consisting of resistance and capacitance, which is seriously dependent on the lamp current, operating frequency, and lamp voltage. A novel soft-starting strategy for pre-heating and igniting the fluorescent lamp is proposed. A half-bridge series-resonant inverter (HB-SRI) is employed as the electronic ballast to verify the system performance. A soft-starting controller (SSC) is implemented to realize zero-voltage switching for the power switches and lower igniting voltage for the lamp. Mathematical model for the lamp before and after firing is built. A design example realized by the HB-SRI is conducted, and the experimental result and the simulation one are close to the theoretical predictions.

1. Introduction

The advent of the high-frequency electronic ballast has contributed great energy saves in our life. Accordingly, the efficiency of fluorescent lamps operating at frequencies above 25kHz is 10-15% more than that at 60Hz[1]. Besides, the electronic ballast also offers numerous advantages better than the magnetic ballast, such as reduced flicker, low audible noise, small size, high power factor, and dimming capability[6]. Generally, the description of the fluorescent lamp is always modeled as a pure resistance after firing[1)-3)]. In fact, this assumption is not true when the fluorescent lamp operates in the high-frequency range[4)-5)]. Furthermore, the starting operation is still the most important task for firing the fluorescent lamp, because it can generate considerable destroy at firing instant to shorten the lamp life. To raise the lamp life, researchers suggest lots of soft starting methods including supplying a low voltage (about 3.5V) for the filament or shorting the starting capacitor on the lamp to heat the filaments approximately at 850 °C in 1.1 seconds[9]. The objective of this paper is to develop a pre-heating control strategy and find a complete model of the fluorescent lamp in high-frequency operation.

The important feature of the lamp under nominal operating conditions is also outlined. The proposed new soft-starting strategy for pre-heating the filament can soft-start the fluorescent lamp and reduce its starting voltage. The pre-heating strategy is realized by a high-frequency resonant inverter driven by a variable frequency train from high to low. The organization of this paper is as follow. Section II presents the modeling of the fluorescent lamp. Section III analyses the half-bridge series-resonant inverter for the fluorescent lamp. The pre-heating strategy of the soft-starting is outlined in section IV. In section V, a design example is conducted, and its experimental results are compared with the computer simulations with the aforementioned model of the fluorescent lamp in section VI. The final section summarizes the conclusion.

2. Modeling the Fluorescent Lamp

The construction of the fluorescent lamp is formed by plasma fulfilled in the tube as shown in Fig. 1. With gas-discharging phenomenon, plasma ionization is built between the two electrodes of the lamp and then achieves luminance in the fluorescent lamp[10)-11)].

The lamp in normal operation (full luminance) behaviors almost a pure resistor; but its impedance is seriously changed out of full luminance due to the operation frequency changed.

Due to the physical similarity as a capacitor, the fluorescent lamp inherently includes capacitance and is significant in the high-frequency range[4)-5)]. In this paper, a half-bridge series-resonant inverter (HB-SRI) is used as the ballast to explore the characteristic of the fluorescent lamp in high-frequency operation. The lamp is parallel-loaded in the HB-SRI. The series resonant tank in HB-SRI consists of a starting capacitor C_s across the lamp and a inductor L_r. The circuit of the presented ballast is configured in Fig. 2. The test scheme for finding the relative parameters of the lamp characteristics is outlined in Fig. 3, in which a universal power analyzer is used to measure the resistance and reactance (R+jX) in the fluorescent lamp. The capacitance of the lamp can then be acquired from the measured X. Typically important parameters of the lamp are measured in Fig. 4, in which the lamp resistance and lamp capacitance, lamp voltage and lamp current versus switching frequency are explored. From the test data in Figs. 4a and 4b, we have the description for $R_{\ell p}$,

$$R_{\ell p}(f_s) = 3.96*10^{-14} f_s^4 - 6.23*10^{-9} f_s^3 + 3.64*10^{-4} f_s^2 - 9.38 f_s + 8.98*10^4 \quad (1)$$

and $C_{\ell p}$ as

$$C_{\ell p}(f_s) = -2.01*10^{-26} f_s^4 + 2.94*10^{-21} f_s^3 - 1.56*10^{-16} f_s^2 + 3.33 f_s - 1.76*10^{-8} \quad (2)$$

Remarkably, the lamp capacitance $C_{\ell p}$ is seriously dependent on the operating point of the lamp and is a function of the lamp current, operating frequency, and lamp voltage. Thus, the impedance of the fluorescent lamp is really frequency- and current-dependent after firing. The explored capacitive behavior in the lamp will affect the generating ignition voltage across the two electrodes of the lamp by changing the parallel capacitance (combining with C_s) on the lamp. The proposed model is then of advantage in high-frequency application.

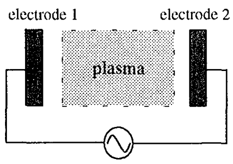

Fig. 1 The configuration of gas-discharging lamp.

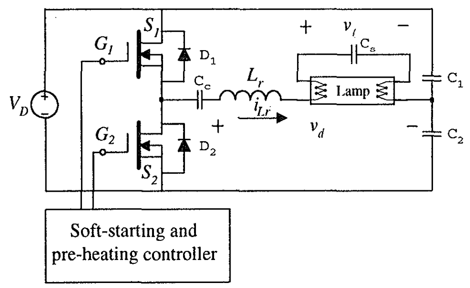

Fig. 2 Circuit topology of HB-SRI electronic ballast with soft-starting and pre-heating controller.

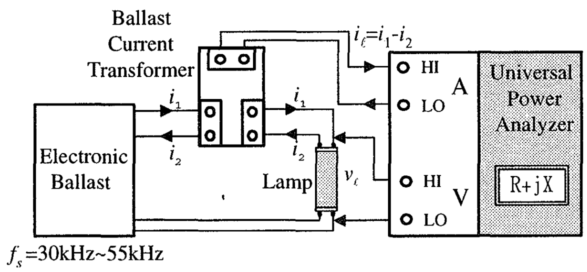

Fig. 3 Test scheme for finding the impedance of the fluorescent lamp.

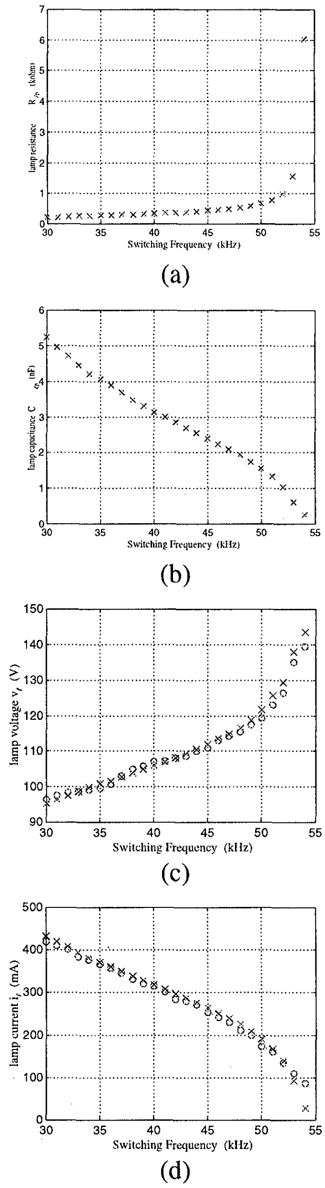

Fig. 4 Measured characteristics of a typical FL 40D-EX/38 fluorescent lamp with respect to the operating frequency, (a) lamp impedance, (b) lamp capacitance, (c) lamp voltage, and (d) lamp current (measurement: xxx, simulation: ooo).

The equivalent circuits of the electronic ballast before and after firing are respectively depicted in Fig. 5[4)-5)]. In Fig. 5, the driving voltage $v_d(t)$ from the switching devices (S_1 and S_2) can be defined as

$$v_d(t) = \begin{cases} V_d, & 0 \le t < \dfrac{\pi}{\omega_s} \\ -V_d, & \dfrac{\pi}{\omega_s} \le t \le \dfrac{2\pi}{\omega_s} \end{cases} \quad (3)$$

Before firing, the lamp behaves high impedance and only the lamp filament resistance r_f is considered in series with C_s. The equivalent circuit in Fig. 5a has the input impedance Z_{i1},

$$Z_{i1} = R_f + j\left(\omega L_r - \frac{1}{\omega C_s}\right) \tag{4}$$

where $R_f = 2r_f$, C_s = starting capacitor. In this case, the resonant frequency ω_{r1} before firing can be given by

$$\omega_{r1} = \frac{1}{\sqrt{L_r C_s}} \tag{5}$$

The circuit quality factor Q_1 is given by

$$Q_1 = \frac{\omega_{r1} L_r}{R_f} = \frac{1}{\omega_{r1} C_s R_f} \tag{6}$$

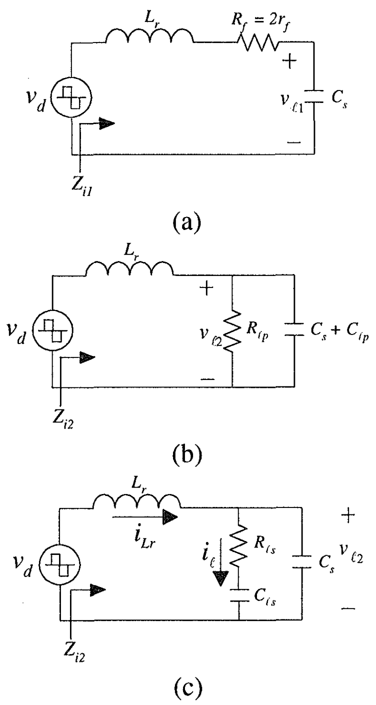

Fig. 5 The equivalent circuit models of the fluorescent lamp (a) before firing, (b) after firing with $R_{\ell p}//C_{\ell p}$ model and (c) after firing with $R_{\ell s}$-$C_{\ell s}$ model.

The peak voltage $V_{\ell 1}$ of the lamp starting voltage $v_{\ell 1}(t)$ on the starting capacitance C_s can be estimated as $V_{\ell 1}=Q_1 V_d$ at resonance, in which $V_d=(4/\pi)(V_D/2)$. Remarkably, the maximum starting voltage for firing the lamp is seriously dependent on the physical geometry of the lamp. The normalized magnitude of the lamp starting voltage $v_{\ell 1}(t)$ to a constant amplitude driving voltage $v_d(t)$ can be given by

$$\left|\frac{V_{\ell 1}(j\omega)}{V_d(j\omega)}\right| = \left|\frac{1}{(1-\omega^2 L_r C_s) + j\omega R_f C_s}\right| = \left|\frac{-jQ_1\left(\frac{\omega_{r1}}{\omega}\right)}{1+jQ_1\left(\frac{\omega}{\omega_{r1}} - \frac{\omega_{r1}}{\omega}\right)}\right| \tag{7}$$

After firing, the equivalent circuit of the fluorescent lamp can be described as either a series form of $R_{\ell s}$-$C_{\ell s}$ or a parallel form of $R_{\ell p}//C_{\ell p}$ as shown in Figs. 5b and 5c, respectively. For parallel combination, the input impedance Z_{i2} in Fig. 5b can be described as

$$\begin{aligned} Z_{i2} &= j\omega L_r + R_{\ell p} // \frac{1}{j\omega(C_{\ell p}+C_s)} \\ &= j\omega L_r + \frac{R_{\ell p}}{1+j\omega R_{\ell p} C_s'} \end{aligned} \tag{8}$$

where

$$R_{\ell p} = R_{\ell s} + \frac{1}{\omega^2 C_{\ell s}^{\,2} R_{\ell s}} \tag{9}$$

$$C_{\ell p} = \frac{C_{\ell s}}{1+\omega^2 C_{\ell s}^{\,2} R_{\ell s}^{\,2}} \tag{10}$$

$$C_s' = C_s + C_{\ell p} \tag{11}$$

The resonant frequency ω_{r2} after firing can then be expressed as

$$\omega_{r2} = \frac{1}{\sqrt{L_r\left[\frac{1+\omega^2 R_{\ell p}^{\,2}(C_{\ell p}+C_s)^2}{\omega^2 R_{\ell p}^{\,2}(C_{\ell p}+C_s)}\right]}} \tag{12}$$

Since the lamp equivalent $R_{\ell p}$ and $C_{\ell p}$ are frequency-dependent, the resonant frequency ω_{r2} would be a variable and not a constant. Fig. 6 shows the relation of the resonant frequency versus the switching frequency, in which the resonant frequency is not constant at luminance and varies in proportion to the switching frequency. The circuit quality factor Q_2 in nominal luminance is then given by

$$\begin{aligned} Q_2 &= \frac{\omega_{r2} L_r\left[1+\omega^2 R_{\ell p}^2 (C_{\ell p}+C_s)^2\right]}{R_{\ell p}} \\ &= \frac{\omega^2 R_{\ell p}(C_{\ell p}+C_s)}{\omega_{r2}} \end{aligned} \tag{13}$$

In this case, the normalized magnitude of the lamp voltage $v_{\ell 2}(t)$ in steady state to a constant amplitude driving voltage $v_d(t)$ can be described as

$$\begin{aligned} \left|\frac{V_{\ell 2}(j\omega)}{V_d(j\omega)}\right| &= \left|\frac{1}{\left[1-\omega^2 L_r (C_{\ell p}+C_s)\right] + j\frac{\omega L_r}{R_{\ell p}}}\right| \\ &= \left|\left\{ \left[1-\frac{Q_2^2}{1+\omega^2 R_{\ell p}^2 (C_{\ell p}+C_s)^2}\right] + j\left(\frac{\omega}{\omega_{r2}}\right)\left[\frac{Q_2}{1+\omega^2 R_{\ell p}^2 (C_{\ell p}+C_s)^2}\right] \right\}^{-1}\right| \end{aligned} \tag{14}$$

The lamp voltages of the HB-SRI electronic ballast in frequency domain before and after firing are shown in Fig. 7a and 7b, respectively. Fig. 7a is for pre-heating the lamp filament. The pre-heating frequency can be set in the high-frequency range such as from 120kHz near to 40kHz, where is the resonant frequency. But for Fig. 7b is for nominal operation, the switching frequency is always set larger than the resonant frequency ω_{r2}.

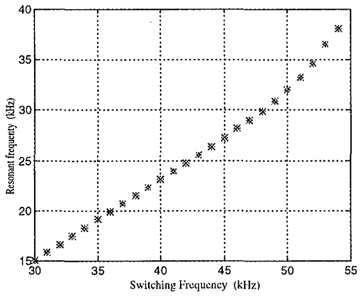

Fig. 6 The switching frequency versus resonant frequency after firing.

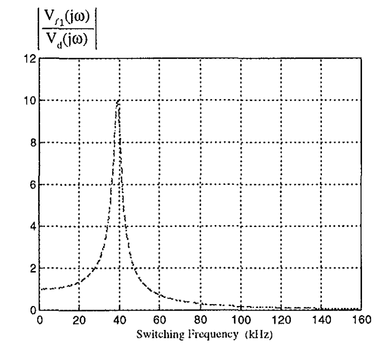

(a)

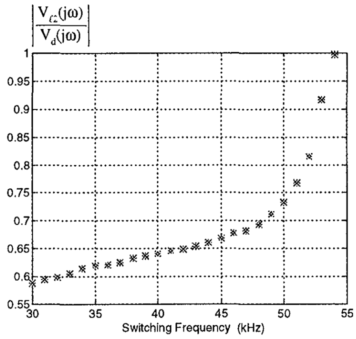

(b)

Fig. 7 Normalized frequency responses of the HB-SRI electronic ballast (a) before firing and (b) after firing.

3. Half-Bridge Series-Resonant Inverter for the Fluorescent Lamp

The presented HB-SRI in nominal luminance has four resonant modes including two charging states and two zero-voltage transition states during one switching cycle. The HB-SRI is operated at continuous-conduction mode (CCM) with the switching frequency higher than the resonant one ω_{r2} [1)-2)]. The equivalent circuits and resonant states are depicted in Fig. 8. Their waveforms with respect to the four modes are shown in Fig. 9. The steady-state resonant behaviors to the four equivalent circuits are respectively described in the following.

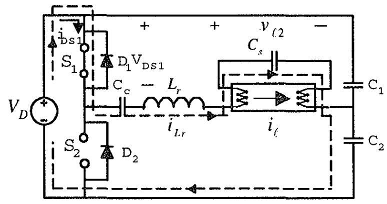

(a)

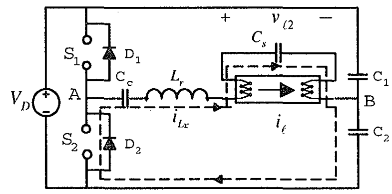

(b)

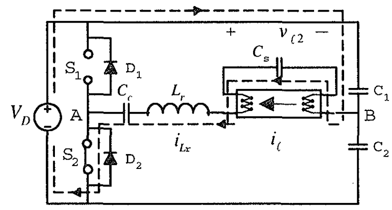

(c)

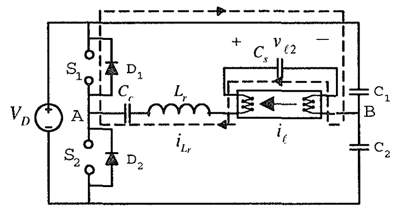

(d)

Fig. 8 Four equivalent circuits of HB-SRI electronic ballast for (a) mode 1 $[t_0, t_1]$, forward charging state, (b) mode 2 $[t_1, t_2]$, zero-voltage transition state, (c) mode 3 $[t_2, t_3]$, reverse charging state, (d) mode 4 $[t_3, t_4]$, zero-voltage transition state•

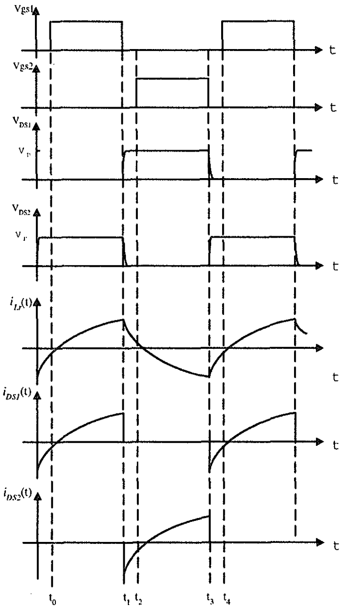

Fig. 9 The simulated resonant waveforms of v_{DS} and i_{Lr}.

1) Mode 1 $[t_0, t_1]$: Forward charging state

As shown in Fig. 8a, when S_1 is on and S_2 is off, the ballast current $i_{Lr}(t)$ is charging through the lamp and the starting capacitor C_s. The ballast current $i_{Lr}(t)$, lamp current $i_\ell(t)$, and lamp voltage $v_{\ell 2}(t)$ across the lamp are given by

$$i_{Lr}(t) = \frac{V_d}{R_{\ell p}} + \left[-\frac{V_d}{R_{\ell p}} + i_{Lr}(t_0)\right]e^{-\alpha t}\cos\omega_d t + \left[-\frac{\alpha V_d}{R_{\ell p}} + \alpha i_{Lr}(t_0) + \frac{V_d - v_{C_s'}(t_0)}{L_r}\right]\frac{e^{-\alpha t}}{\omega_d}\sin\omega_d t \qquad (15)$$

$$i_\ell(t) = \frac{V_d}{R_{\ell p}} + 2\alpha\left[R_{\ell p}C_{\ell p}i_{Lr}(t_0) + C_s v_{C_s'}(t_0) - V_d C_s'\right]e^{-\alpha t}\cos\omega_d t + \beta_1 e^{-\alpha t}\sin\omega_d t \qquad (16)$$

where

$$\beta_1 = \frac{1}{\omega_d}\left\{\begin{matrix}\omega_0^2 C_{\ell p}\left(V_d - v_{C_s'}(t_0)\right) \\ +2\alpha^2\left[i_{Lr}(t_0)R_{\ell p}\left(2C_s' - C_{\ell p}\right) - C_s v_{C_s'}(t_0) - V_d C_s'\right]\end{matrix}\right\} \qquad (17)$$

and

$$v_{\ell 2}(t) = v_{C_s'}(t) = V_d + \left[-V_d + v_{C_s'}(t_0)\right]e^{-\alpha t}\cos\omega_d t + \left[-\alpha V_d - \alpha v_{C_s'}(t_0) + \frac{i_L(t_0)}{C_s'}\right]\frac{e^{-\alpha t}}{\omega_d}\sin\omega_d t \qquad (18)$$

where the damped frequency $\omega_d = \sqrt{\omega_o^2 - \alpha^2}$, corner frequency $\omega_o = 1/\sqrt{L_r C_s'}$ and the damping factor $\alpha = 1/2R_{\ell p}C_s'$

2) Mode 2 $[t_1, t_2]$: Zero-voltage transition state

Since the switching frequency of the ballast is designed to operate at the frequency higher than the resonant one, S_1 turns off when $i_{Lr}(t)$ reaches to a nominal value as shown in Fig. 9. During the turn-off interval of both two switches S_1 and S_2, the inductor current $i_{Lr}(t)$ will then free-wheel through the body diode D_2 as shown in Fig. 8b. It provides a zero voltage across switch S_2 before its turn-on while the $i_{Lr}(t)$, $i_\ell(t)$, and $v_{\ell 2}(t)$ can be described as

$$i_{Lr}(t) = \frac{-V_d}{R_{\ell p}} + \left[\frac{V_d}{R_{\ell p}} + i_{Lr}(t_1)\right]e^{-\alpha t}\cos\omega_d t + \left[\frac{\alpha V_d}{R_{\ell p}} + \alpha i_{Lr}(t_1) + \frac{-V_d - v_{C_s'}(t_1)}{L_r}\right]\frac{e^{-\alpha t}}{\omega_d}\sin\omega_d t \qquad (19)$$

$$i_\ell(t) = 2\alpha\left[R_{\ell p}C_{\ell p}i_{Lr}(t_1) + C_s v_{C_s'}(t_1)\right]e^{-\alpha t}\cos\omega_d t + \beta_2 e^{-\alpha t}\sin\omega_d t \qquad (20)$$

where

$$\beta_2 = \frac{2\alpha}{\omega_d}\left\{i_{Lr}(t_1) - \frac{R_{\ell p}C_{\ell p}v_{C_s'}(t_1)}{L_r} - \alpha\left(R_{\ell p}C_{\ell p}i_{Lr}(t_1) + C_s v_{C_s'}(t_1)\right)\right\} \qquad (21)$$

and

$$v_{\ell 2}(t) = -V_d + \left[V_d + v_{C_s'}(t_1)\right]e^{-\alpha t}\cos\omega_d t + \left[\alpha V_d - \alpha v_{C_s'}(t_1) + \frac{i_{Lr}(t_1)}{C_s'}\right]\frac{e^{-\alpha t}}{\omega_d}\sin\omega_d t \qquad (22)$$

3) Mode 3 $[t_2, t_3]$: Reverse charging state

During the mentioned free-wheeling state, S_2 turns on at zero-voltage switching. The ballast current $i_{Lr}(t)$ is then reversely charging through the lamp and the starting capacitor C_s. The $i_{Lr}(t)$, $i_\ell(t)$, and $v_{\ell 2}(t)$ can be given by

$$i_{Lr}(t) = -\frac{V_d}{R_{\ell p}} + \left[\frac{V_d}{R_{\ell p}} + i_{Lr}(t_2)\right]e^{-\alpha t}\cos\omega_d t + \left[\frac{\alpha V_d}{R_{\ell p}} + \alpha i_{Lr}(t_2) + \frac{-V_d - v_{C_s'}(t_2)}{L_r}\right]\frac{e^{-\alpha t}}{\omega_d}\sin\omega_d t \qquad (23)$$

$$i_\ell(t) = -\frac{V_d}{R_{\ell p}} + 2\alpha\left[R_{\ell p}C_{\ell p}i_{Lr}(t_2) + C_s v_{C_s'}(t_2) + V_d C_s'\right]e^{-\alpha t}\cos\omega_d t + \beta_3 e^{-\alpha t}\sin\omega_d t \qquad (24)$$

where

$$\beta_3 = \frac{1}{\omega_d}\left\{\begin{matrix}\omega_0^2 C_{\ell p}\left(-V_d - v_{C_s'}(t_2)\right) \\ +2\alpha^2\left[i_{Lr}(t_2)R_{\ell p}\left(2C_s' - C_{\ell p}\right) - C_s v_{C_s'}(t_2) - V_d C_s'\right]\end{matrix}\right\} \qquad (25)$$

and

$$v_{\ell 2}(t) = -V_d + \left[V_d + v_{C_s'}(t_2)\right]e^{-\alpha t}\cos\omega_d t + \left[\alpha V_d - \alpha v_{C_s'}(t_2) + \frac{i_{Lr}(t_2)}{C_s'}\right]\frac{e^{-\alpha t}}{\omega_d}\sin\omega_d t \qquad (26)$$

4) Mode 4 $[t_3, t_4]$: Zero-voltage transition state

When S_2 turns off at $t = t_3$, the ballast current $i_{Lr}(t)$ is free-wheeling again through the body diode D_1 as shown in Fig. 8d. The $i_{Lr}(t)$, $i_\ell(t)$ and $v_{\ell 2}(t)$ can be expressed as

$$i_{Lr}(t) = \frac{V_d}{R_{\ell p}} + \left[\frac{-V_d}{R_{\ell p}} + i_{Lr}(t_3)\right]e^{-\alpha t}\cos\omega_d t + \left[-\frac{\alpha V_d}{R_{\ell p}} + \alpha i_{Lr}(t_3) + \frac{V_d - v_{C_s'}(t_3)}{L_r}\right]\frac{e^{-\alpha t}}{\omega_d}\sin\omega_d t \qquad (27)$$

$$i_\ell(\mathrm{t}) = 2\alpha\left[R_{\ell p}C_{\ell p}i_{Lr}(\mathrm{t}_3) + C_s v_{C_s'}(\mathrm{t}_3)\right]e^{-\alpha t}\cos\omega_d t + \beta_4 e^{-\alpha t}\sin\omega_d t \tag{28}$$

where

$$\beta_4 = \frac{2\alpha}{\omega_d}\left\{i_{Lr}(\mathrm{t}_3) - \frac{R_{\ell p}C_{\ell p}v_{C_s'}(\mathrm{t}_3)}{L_r} - \alpha\left(R_{\ell p}C_{\ell p}i_{Lr}(\mathrm{t}_3) + C_s v_{C_s'}(\mathrm{t}_3)\right)\right\} \tag{29}$$

and

$$v_{\ell 2}(\mathrm{t}) = V_d + \left[-V_d + v_{C_s'}(\mathrm{t}_3)\right]e^{-\alpha t}\cos\omega_d t + \left[-\alpha V_d - \alpha v_{C_s'}(\mathrm{t}_3) + \frac{i_L(\mathrm{t}_3)}{C_s'}\right]\frac{e^{-\alpha t}}{\omega_d}\sin\omega_d t \tag{30}$$

Substituting (1)-(2) into (15)-(30), we have the simulation results of lamp voltage $v_{\ell 2}(t)$ and lamp current $i_\ell(t)$ versus operating frequency as shown in Figs. 4c and 4d. Accordingly, the complete resonant waveforms of v_{DS} (t) and $i_{Lr}(t)$ are simulated and displayed in Fig. 9.

4. Pre-Heating Strategy for HB-SRI Fluorescent Lamp

Generally, the electronic ballast system so far requires a higher starting voltage to ignite the fluorescent lamp. It then results in high voltage stress, higher EMI to shorten the life of the lamp[6)-8)]. To reduce the highly impact upon the lamp, a soft-starting controller (SSC) for gradually firing the fluorescent lamp is proposed. The system diagram of the control strategy is shown in Fig 10. The presented SSC consists of a voltage-in ramp generator (VIRG), a voltage-controlled oscillator (VCO), a pre-heating and firing control timer, and a driver with dead-time control. The realization circuit of the SSC is shown in Fig. 11a, in which the voltage-in ramp wave from VIRG is applied to the VCO to produce a triangular wave with variable frequency from high to low, as shown in Fig. 11b. The output of the VCO then splits into two control signals with proper dead-time for gating the power switches as shown in Figs. 11a and 11b, whose truth table is shown in Fig. 11c. The variable voltage V_R in Fig. 11b is used to adjust a proper dead-time between the two control signals formed by a D Filp-Flop. The strategy of the SSC is to initiate the lamp with a variable frequency from high to low, which assures that the pre-heating process is gradually achieved. As the operating frequency of the SSC is close to the resonant frequency ω_{r1}, the lamp voltage will then rise up to the igniting level to fire the fluorescent lamp. The required igniting voltage for the lamp is strictly dependent the pre-heating profile from the SSC.

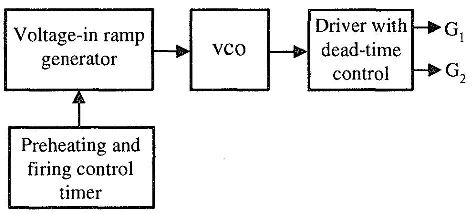

Fig. 10 The structure of the soft-starting controller (SSC).

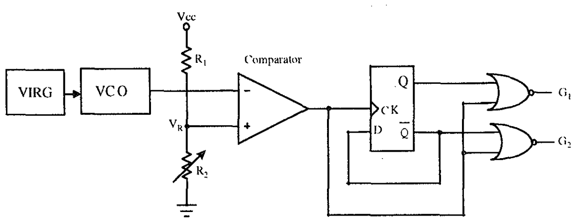

(a)

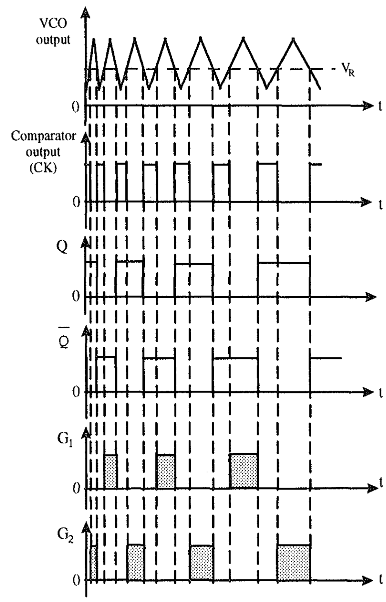

(b)

D	CK	Q_{n+1}	$\overline{Q_{n+1}}$	$G_1 = \overline{Q_{n+1} + CK}$	$G_2 = \overline{\overline{Q_{n+1}} + CK}$
0	0	Q_n	$\overline{Q_n}$	$\overline{Q_n}$	Q_n
0	1	0	1	0	0
1	0	Q_n	$\overline{Q_n}$	$\overline{Q_n}$	Q_n
1	1	1	0	0	0

(c)

Fig. 11 (a) The realized circuit of the SSC, (b) gate pulses for the power switches, and (c) truth table of the dead time control.

5. Design considerations

According to the aforementioned analysis, we can find the relative parameters from Fig. 4 with the considerations of the required lamp current, lamp voltage, and switching frequency. In this paper, a prototype of a 40W electronic ballast with soft-starting control is designed and realized. We use a fluorescent lamp FL-40D/38 produced from China Electric Mfg. Corp. as the experimental target. From the data sheets, we find that the lamp current is 410mA at rated power of 38W. In this design, we preset the rated output power is 35W and from Figs. 4c and 4d, the relative data are lamp rms current I_ℓ=330mA, lamp rms voltage V_ℓ=105V, and operating frequency f_s=39kHz. The specifications are given in the following: input dc voltage V_D=380V from a PFC with power factor$\geq$0.95, operating frequency of the

SSC initiating from 100kHz→50kHz, starting voltage $550V_{p\text{-}p}$, nominal operating frequency 39kHz, temperature rise below 30°C, current crest factor <1.7, total harmonic distortion ≤ 15%. Firstly, we preset the switching frequency for firing the lamp is at f_s=50kHz and we let the required starting voltage be $550V_{p\text{-}p}$, The filament resistance r_f=4~6Ω and would be 4~5 times after heating, and we presume R_f =50Ω. From (7), we have, in starting state,

$$\left|\frac{V_{\ell 1}(j\omega)}{V_d(j\omega)}\right| = \frac{550/2}{\frac{4}{\pi}\frac{380}{2}} = 1.14 = \frac{1}{\sqrt{\left[1-\omega^2 L_r C_s\right]^2 + \left[\omega R_f C_s\right]^2}} \qquad (31)$$

After firing and in normal operation, we have found the equivalent parallel impedance $R_{\ell p}$=344Ω, and $C_{\ell p}$=3.14nF. From (14), we have, in steady state,

$$\left|\frac{V_{\ell 2}(j\omega)}{V_d(j\omega)}\right| = \frac{105\sqrt{2}}{\frac{4}{\pi}\frac{380}{2}} = 0.62 = \frac{1}{\sqrt{\left[1-\omega^2 L_r\left(C_{\ell p}+C_s\right)\right]^2 + \left[\frac{\omega L_r}{R_{\ell p}}\right]^2}} \qquad (32)$$

Combining (31) and (32), the derived parameters for this design are given by L_r= 2.11 mH (use 2.05mH) and C_s= 8.6 nF (use 8.2nF).

6. Simulation and experimentation

In this paper, a 40W ballast with pre-heating strategy is realized to estimate the performance of the fluorescent lamp and to assess the proposed model. Based on ANSI C82.11, the pre-heating time t_p for a rapid-start ballast should be greater than 500msec. In this design, we assume the required starting time t_p =1 second and use the model of Fig. 5a for evaluating the proposed pre-heating strategy. The frequency for pre-heating the lamp filament is designed changing from 100kHz to 50kHz. Since the filament resistance r_f will increase with the temperature rise, we assume the final filament resistance R_f =4 × $2r_f$. The simulation response of the lamp voltage by Fig. 5a before firing is clearly shown between 0 and 1 second in Fig. 12a. When the lamp fires at t =1 second, by Fig. 5b, the simulation response of the lamp voltage is shown after t ≥1 second in Fig. 12a. The soft-starting lamp voltage is measured in Fig. 12b. The simulation and experiment results are quite the same each other. The actual pre-heating time measured is 1.04 seconds and the starting voltage is only $550V_{p\text{-}p}$. By computation, the resonant frequency is 38.82kHz, the circuit quality factor Q_1 = 41.74 when R_f =50Ω. The lamp current is also measured and shown in Fig. 12c. Due to properly pre-heating, no high current spike occurs at the ignition point.

Furthermore, the proposed ballast can operate in the frequency range from 30kHz→55kHz, in which the corresponding output power changes from 40→12W, the equivalent parallel resistance $R_{\ell p}$ from 225Ω→1.6kΩ, and the equivalent parallel capacitance $C_{\ell p}$ from 5.24nF→0.61nF. With the model of Fig. 5b and the estimated parameters $R_{\ell p}$=672Ω and $C_{\ell p}$=1.57nF at f_s=50kHz, $v_{\ell 2}(t)$ and $i_\ell(t)$ are simulated with (15)-(30) and shown in Fig. 13b. The waveforms of $i_\ell(t)$, $v_{\ell 2}(t)$, and $i_{Lr}(t)$ at f_s=50kHz are measured in Fig. 13c and 13d, respectively. It is clearly seen that the simulation result with the proposed lamp model in Fig. 13b is more close to the measured one in Fig. 13c. There is only small phase difference between $v_{\ell 2}(t)$ and $i_\ell(t)$; but for $v_{\ell 2}(t)$ and $i_{Lr}(t)$, an obvious phase difference exists. Besides, the simulation by the resistive lamp model is also shown in Fig. 13a for comparison and its reality is so different from those shown in Figs. 13b and 13c.

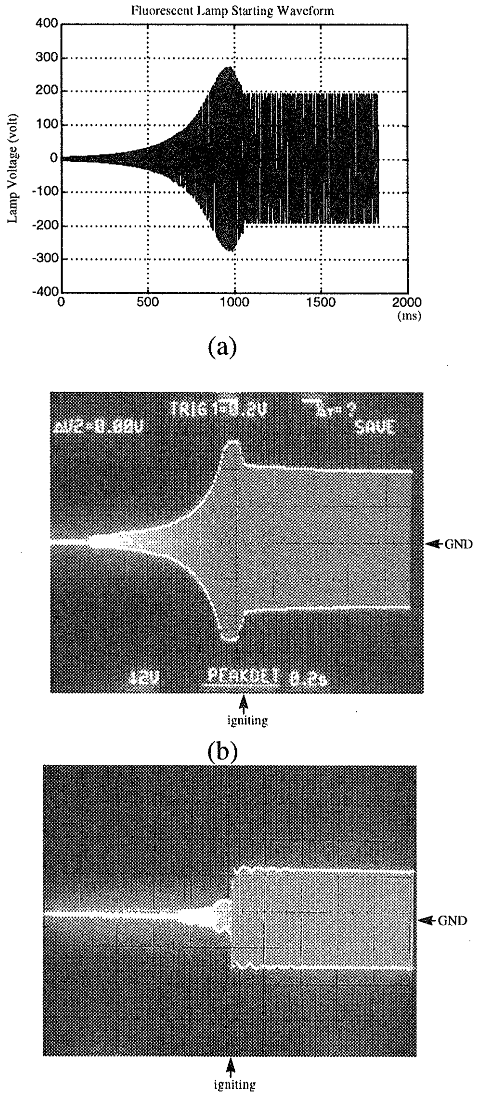

Fig. 12 Starting voltages of the lamp under SSC mode, (a) simulation and (b) experiment, (Ver: 100V/div; Hor: 0.2 sec/div); (c) experimental lamp current (Ver: 200mA/div; Hor : 0.2 sec/div).

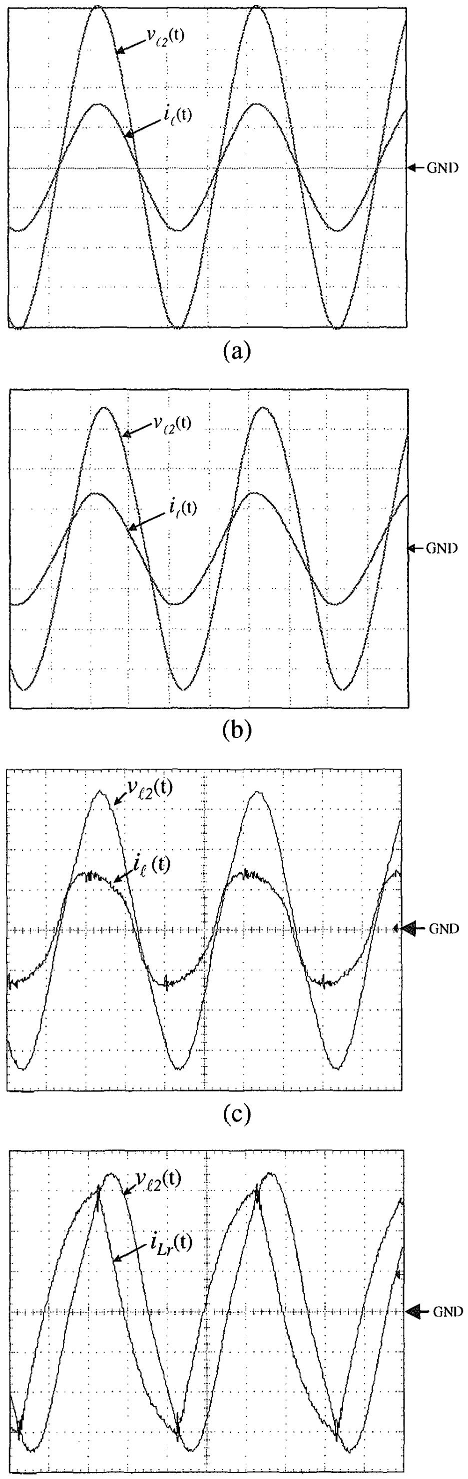

Fig. 13 Under test conditions: L_r= 2.05 mH, C_s= 8.2 nF, and operation frequency = 50kHz, (a) simulation, lamp voltage $v_{\ell 2}$ versus lamp current i_ℓ with general lamp model (R model), (b) simulation, $v_{\ell 2}$ versus i_ℓ with the proposed lamp model ($R_{\ell p}//C_{\ell p}$ model), (c) experiment, $v_{\ell 2}$ versus i_ℓ with $R_{\ell p}//C_{\ell p}$ model, and (d) experiment, lamp voltage $v_{\ell 2}$ versus inductor current i_{Lr} with $R_{\ell p}//C_{\ell p}$ model (Voltage, Ver: 50/div; Current, Ver: 200mA/div, Hor: 5μsec /div).

7. Conclusion

In this paper, a complete model of the fluorescent lamp before and after igniting is proposed. The lamp characterizes an impedance consisting of the resistance and capacitance when operating in high frequency range. A soft-starting strategy is presented for reducing the ignition voltage of the fluorescent lamp. A zero-voltage switching technique is applied to raise the ballast power efficiency. In this paper, a design example realized by the HB-SRI is presented to assess the ballast performance. Due to the pre-heating strategy, the fluorescent lamp can be ignited smoothly under lower starting voltage below $550V_{p\text{-}p}$, which can reduce discoloration of the lamp.

Acknowledgment

The authors wish to thank the National Science Council, Taiwan, R.O.C. for his sponsorship of Project number: NSC86-2213-E-011-078

References

(1) M. K. Kazimierczuk, and W. Szaraniec, "Electronic Ballast for Fluorescent Lamps," *IEEE Trans. Power Electron.*, vol. 8, no. 4, pp. 386-395, Oct. 1993.

(2) M. C. Cosby and R. M. Nelms, " A Resonant Inverter for Electronic Ballast Applications," *IEEE Trans. Ind. Electron.*, vol.41, pp.418-425, Aug. 1994.

(3) R. R. Verderber, O. Morse, and F. M. Rubinatein, "Life of fluorescent lamps operated at high frequencies with solid-state ballasts," *Proc. IEEE IAS'85*, pp. 1724-1728, 1985.

(4) G. C. Hsieh, E. P. Tsai, and P. S. Sung "Experimental Study of the Fluorescent Lamp with An Electronic Dimmer Controller," *The 7th Int'l symp. of the Science & Tech. of Light Sources*, pp. 73-74, Aug. 1995.

(5) G. C. Hsieh, P. S. Sung, and E. P. Tsai " Experimental Modeling of the Fluorescent Lamp," *The 7th Int'l Symp. of the Science & Tech. of Light Sources*, pp.223-224, Aug. 1995.

(6) W. R. Alling, "Important Design Parameters for Solid-State Ballasts," *IEEE Trans. Ind. Electron.*, vol 25, no. 2, pp. 203-207, Mar. 1989.

(7) Y. Ji, and R. Davis, "Starting Performance of High-Frequency Electronic Ballasts for 4-foot Fluorescent Lamps," *IEEE IAS'95*, pp. 2083-2089, 1995.

(8) A. Okude, A. Ueoka, Y. Kambara and M. Mitani, "Development of and Electronic Dimming Ballast for Fluorescent Lamps," *J. of Illuminating Eng. Society*, pp.15-21, Winter 1992.

(9) E. E. Hammer, and T. K. McGowan, "Characteristics of Various F40 Fluorescent Systems at 60Hz and

High-frequency," *IEEE Trans. Ind. Appl.*, vol. IA-21, no.1, pp.11-16, 1985.
(10) F. F. Chen, *Introduction to Plasma Physics*, New York: Plenum Press, 1974.
(11) J. F. Waymouth, Electronic Discharge Lamps, London: The M. I. T. Press, 1971.
(12) American National Standards Institute, *High-frequency fluorescent lamp ballasts*, ANSI C82.11-1993, New York, NY: American National Standards Institute,1993.